UNIVERSITY OF CALIFORNIA
RIVERSIDE

Investigation of Climate Forcing Agents on Tropical Belt Width Through the 21st Century

A Thesis submitted in partial satisfaction
of the requirements for the degree of

Master of Science

in

Geological Sciences

by

Osinachi Franklin Ajoku

June 2014

Thesis Committee:
Dr. Robert Allen, Chairperson
Dr. Roya Bahreini
Dr. Richard Minnich

The Thesis of Osinachi Franklin Ajoku is approved:

Committee Chairperson

University of California, Riverside

ABSTRACT OF THE THESIS

Investigation of Climate Forcing Agents on Tropical Belt Width Through the 21st Century

by

Osinachi Franklin Ajoku

Master of Science, Graduate Program in Geological Sciences
University of California, Riverside, June 2014
Dr. Robert J. Allen, Chairperson

Recent studies suggest that the tropics have expanded from ~2-5° over the past few decades and that this widening may continue into the future in association with global climate change. This expansion has potentially important implications for subtropical societies that include profound changes in the hydrological cycle and large-scale atmospheric circulation. Consistent with theory, models forced by greenhouse gases (GHG's) produce this expansion, however, some measurements have showed that observed tropical expansion is significantly larger than simulations of the 20th and 21st century from the Coupled Model Intercomparison Project version 3 (CMIP3). Recent climate simulations have shown that direct heating of the troposphere and surface, such as that caused by absorbing aerosols can drive expansion.

In this study, we quantify future changes in the tropical belt width using CAM3 and the 4 Representative Concentration Pathway's (RCPs) through the end of the 21st century. The RCP scenarios all assume stringent emissions controls on aerosols and their precursors, and hence include progressive decreases through the 21st century. Changes in

tropical belt width are analyzed using 5 metrics. We find that the global, annual expansion rates vary from .09 +/- .05º and .14 +/- .03º decade^{-1} for GHG and SO_2 forcings respectively under RCP 4.5. Furthermore, Northern hemisphere (NH) expansion rates vary from .05 +/- .04º and .12 +/- .02º decade^{-1} for GHG and SO_2 forcings respectively under RCP 4.5. As widening increases with RCP, SO_2 still accounts for as much widening as GHG's. Given the large reductions in future sulfate emissions with all RCPs reaching preindustrial values by 2100, we find that sulfate aerosols may be just as dominant a driver of tropical expansion in the northern hemisphere as GHG's through the end of the 21st century.

Table of Contents

List of Figures

List of Tables

1. Introduction

The effects of anthropogenic aerosols and greenhouse gases (GHG's) on Earth and its environment remain a growing concern. As their emissions are projected to change, so will the resulting climatic impacts. Future changes in GHG and aerosol emissions will have significant effects on large-scale atmospheric circulation. Changes in the width of the tropical belt can lead to a shift in precipitation and climate patterns. Understanding such a change is important, as a majority of the planet's population lay within these boundaries and is reliant on precipitation for agriculture and water resources.

Several studies suggest that the tropics have expanded by ~2º-5° during the late 20th century (Hu & Fu, 2007) and that this widening may continue into the future in association with anthropogenic climate change. This evidence is based on several metrics, including a poleward shift of the Hadley cell, jet streams, subtropical dry zones, extratropical storm tracks and the latitude at which zonally averaged precipitation P equals zonally averaged evaporation E (Archer and Caldeira, 2008; Zhou et al., 2011; Bender et al., 2011; Quan et al., 2013). This expansion has potentially important implications for subtropical societies and may lead to profound changes in the hydrological cycle. Models forced by GHGs produce this expansion (Seidel et al., 2008; Lu et al., 2007, 2009) and model control runs indicate that the magnitude of the late twentieth-century widening cannot be explained by natural variability alone (Yin, 2005). However, Johanson and Fu (2009) showed that observed tropical expansion is significantly larger than simulations of the 20th and 21st century from the Coupled Model

Intercomparison Project version 3 (CMIP3). Most indices of tropical width indicated poleward trends during the last 30 years. Recent climate simulations have shown that direct heating of the troposphere, such as that caused by absorbing aerosols or tropospheric ozone can drive expansion (Allen & Sherwood, 2011). Moreover, reductions in reflecting aerosols, such as sulfate, may lead to expansion of the tropical belt by a similar mechanism. Given the large reductions in future sulfate emissions; with all Representative Concentration Pathways (RCPs) reaching preindustrial values by 2100, sulfate aerosols may be the dominant driver of tropical expansion through the 21st century. Furthermore, future changes in anthropogenic aerosols, including a progressive decrease in sulfates (SO_2) pose the highest risk at shifting precipitation amounts due to its negative radiative forcing in the atmosphere.

This research proposes to quantify the effect that anthropogenic forcing agents have in expanding tropical belt width through the 21st century using all RCPs. Specifically, this research will address how the rate of aerosol emission reductions and GHG increases will alter the width of the tropical belt and how these rates vary with RCP. Important questions that this research will attempt to answer include: 1) How do anthropogenic aerosols compare against GHGs in perturbing the planet's hydrological cycle; 2) how do anthropogenic aerosols compare to GHGs in affecting the expansion of tropical boundaries, and 3) what effect will future aerosol and GHG emission changes have on the hydrological cycle?

This research will be the first to quantify future changes in the tropical belt width and explore the relative roles of GHGs and aerosols in driving these changes through the

21st century. This work will yield a better understanding of how emission reductions of short-lived pollutants may have unexpected impacts on large-scale atmospheric circulation and the hydrological cycle. Understanding such changes, especially precipitation, will be useful for third-world and developing countries at risk of drought or dependent on precipitation for water resources and local agricultural yields. Of particular concern are the semi-arid regions poleward of the subtropical dry belts, including the Mediterranean, the southwestern United States and northern Mexico, southern Australia, southern Africa and parts of South America (Frierson and Lu, 2007).

2. Methods

This chapter will discuss all of the data sources utilized, how the data was analyzed, as well as the methods used for statistical analysis and their contribution to the study.

2.1 Model Description and Experimental Design

This research utilized monthly-mean output data created by a simulation from the National Center of Atmospheric Research's (NCAR's) Community Atmosphere Model version 3 (CAM3). This model is the fifth generation of the NCAR atmospheric global climate model (GCM). CAM3 was run at T42 resolution (2.8° by 2.8° grid) and 26 hybrid vertical pressure levels coupled to the Community Land Model (CLM) version 3, a slab ocean-thermodynamic sea ice model, and the Snow, Ice and Aerosol Radiative (SNICAR) model (Flanner et al., 2007; Bond & Bergstrom, 2006) for the period 2000-2099. In addition to the usual natural forcings, this run included radiatively active black carbon in the atmosphere and snow and an enhancement factor of 1.5 for solar absorption by coated hydrophilic particles (Flanner et al., 2007, 2009). Aerosol Indirect effects were not included. This work shows results from CAM3 integrated from initial conditions based on a 30-year control simulation with constant 2000 forcing.

2.1.1 CAM3 Description

The Community Atmospheric Model (CAM) is a global atmospheric general circulation model developed from the NCAR Community Climate Model version 3 (CCM3) (Lipscomb & Sacks, 2010**)**. Contrasting to previous versions, CAM3 was designed through collaborative process with users and developers in the Atmospheric Model Working Group (AMWG). The AMWG preserved the spectral Eulerian dynamical core with the option to run CAM3 with semi-Lagrange dynamics or with finite-volume dynamics. The parameterization for deep convective used in this model was adopted from Zhang and McFarlane (1995). This scheme ultimately assumes that convective scale updrafts may exist whenever the atmosphere is conditionally unstable in the lower troposphere.

Some of the physics incorporated in CAM3 include: (1) Treatment of cloud-condensed water using a prognostic treatment; (2) A replacement of uniform background aerosol with a present-day climatology of sulfate, sea-salt, carbonaceous and soil-dust aerosols; (3) Evaporation of convective precipitation and (4) Clean separation between the physics and dynamics (Collins, 2004).

2.2 Data Integration

Time-varying forcing followed the recently developed CMIP5 data set, including estimated concentrations of GHG's and primary emissions of sulphur dioxide and black carbon. Future concentration estimates were derived from the four RCPs used by the

Intergovernmental Panel on Climate Change (IPCC) for the Fifth Assessment Report (AR5). These RCPs complement and, for some purposes, are meant to replace earlier scenario-based projections of atmospheric composition, such as those from the Special Report on Emissions Scenarios (SRES; Nakicenovic and Swart 2000). The four RCPs span a range of radiative forcing values, i.e. from 2.6 to 8.5 W/m^2 by the end of the 21^{st} century. The radiative forcing estimates are based on the forcing of greenhouse gases and other forcing agents, not including land use (albedo) or dust and nitrate aerosols. [The RCPs provide a unique set of data, particularly with respect to comprehensiveness and detail, as well as spatial scale of information for climate model projections. These 4 scenarios are the product of innovative collaboration between integrated assessment modelers, climate modelers, terrestrial ecosystem modelers and emission inventory experts (Vuuren et al., 2011)].

2.2.1 Representative Concentration Pathways

The four RCPs included in CAM3 were created for the climate modeling community in order to conduct near-term (30 years) and long-term (100 years) modeling experiments. These scenarios represent expert judgments regarding credible future emissions based on research into socioeconomic, environmental, and technological trends represented in integrated assessment models, with a focus on energy and land-use patterns. The word 'representative' signifies that each RCP provides only one of many possible scenarios that would lead to the specific radiative forcing value. The term 'pathway' emphasizes that not only the long-term concentration levels are of interest, but

also the trajectory taken over time to reach that outcome (Moss et al.). As stated earlier, the radiative forcing values associated with the RCPs range from 2.6 to 8.5 W/m^2. RCPs 2.6 and 4.5 are representative of the lowest and intermediate mitigation scenarios respectively, RCP 6.0 can be considered as either a medium baseline or a high mitigation case, while RCP 8.5 is the high emission scenario.

Scenario Component	RCP2.6	RCP4.5	RCP6	RCP8.5
Greenhouse gas emissions	Very low	Medium-low mitigation Very low baseline	Medium baseline; high mitigation	High baseline
Agricultural area	Medium for cropland and pasture	Very low for both cropland and pasture	Medium for cropland but very low for pasture (total low)	Medium for both cropland and pasture
Air pollution	Medium-Low	Medium	Medium	Medium-high

Table 1. **RCP Characteristics**. Table describes changes of various components for each RCP (Vuuren et al., 2011).

Each RCP includes time-varying loads for aerosols and volume mixing ratios for GHG's (i.e. CO_2, O_3, CH_4, N_2O, chlorofluorocarbon's and hydro fluorocarbon's) (Vuuren et al., 2011). All four RCPs have large decreases in anthropogenic aerosols. Figure 1 shows CO_2 volume mixing ratio for the years 2000-2099 used in this study. For RCP 2.6, CO_2 emissions peak at ~420 ppm before returning to modern day levels of 400 ppm. RCPs 4.5 and 6.0 follow the same emission trajectory up until ~2060 before changes are assumed to be made with mitigation. These scenarios eventually reach 545 and 675 ppm respectively. CO_2 emissions under RCP 8.5 reflect a steady growth curve with a volume

mixing ratio value of ~940 ppm by the end of the century. Table 1 lists the main characteristics of each RCP.

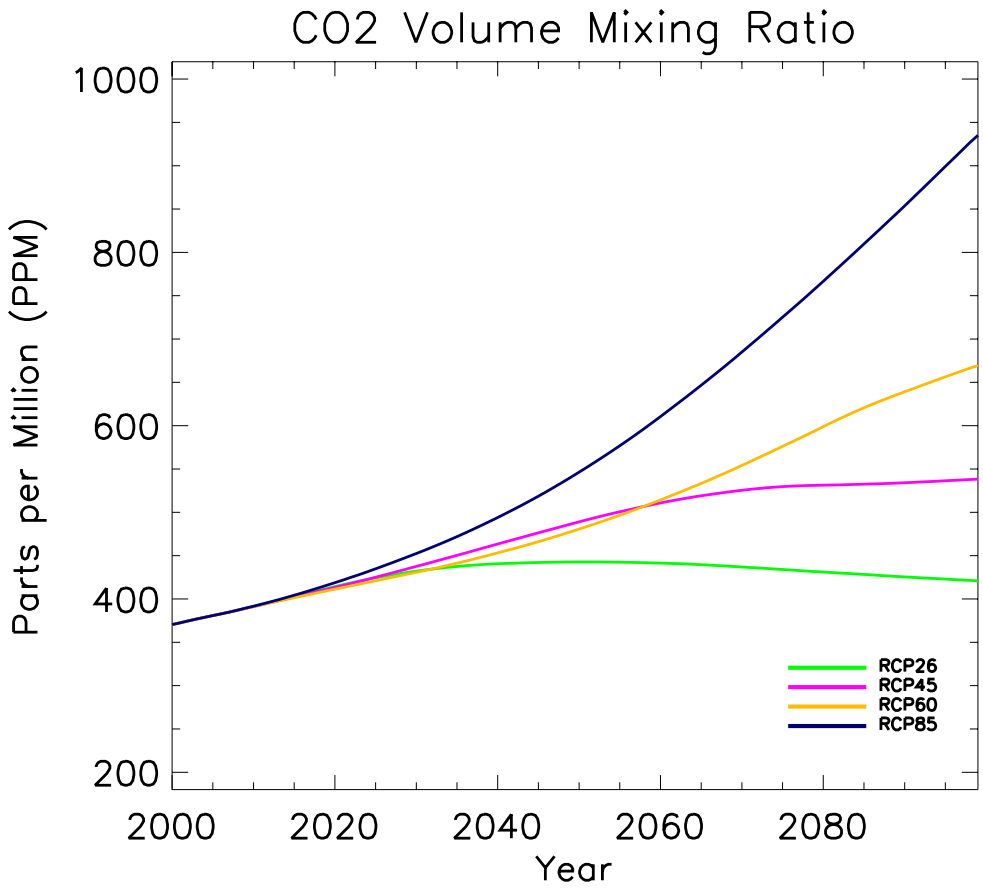

Figure 1. CO_2 Volume Mixing Ratio (2000-2099). This figure represents a time-series of CO_2 evolution through the 21st century for each RCP.

2.3 Data Analysis

2.3.1 Experimental Design

All data analyzed under each RCP was categorized by forcing agents. Data using all forcing agents (ALL) included GHG's, Sulfur Dioxide (SO_2), BC, tropospheric ozone

and organic carbon. GHG-only or aerosol-only forcing's were computed by subtracting a specific run from the run with ALL forcing's (i.e. ALL-NO_BC = BC-only forcing). Allen et al. (2012) shows the importance of non-GHG forcings towards widening the tropics, including heterogeneous warming agents in the NH. This study focuses only on GHG, SO_2, BC and ALL forcings. Figures 2 and 3 show the mass column loads for sulfate and BC aerosols respectively.

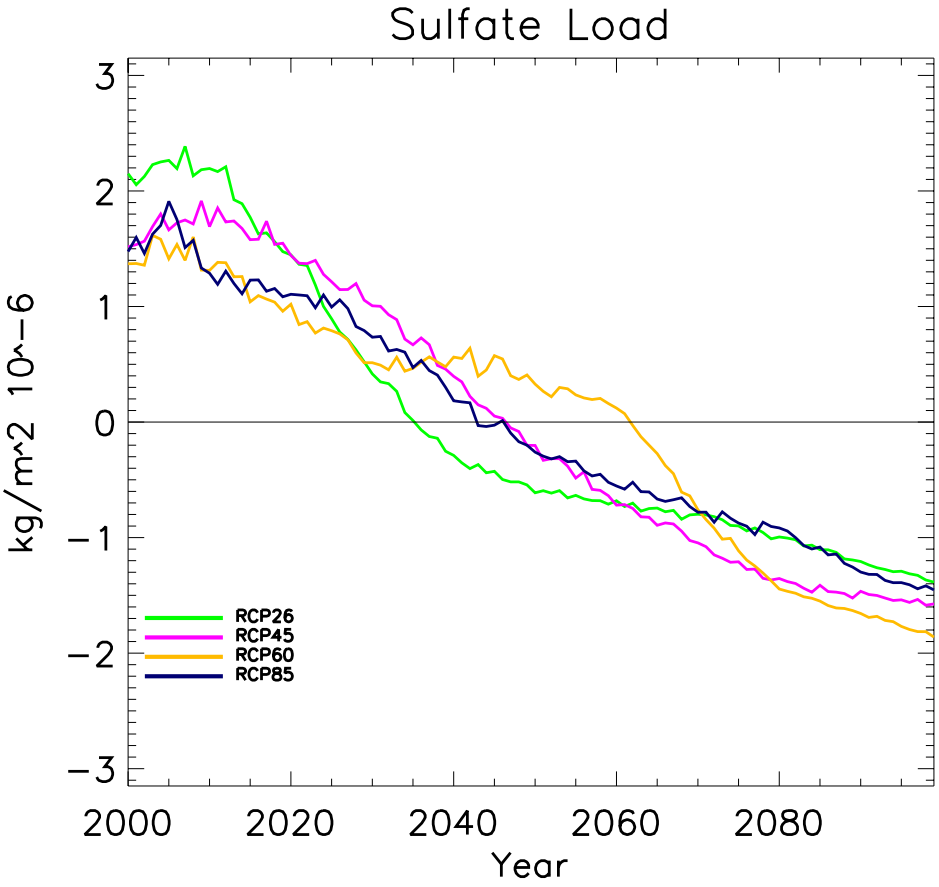

Figure 2. Sulfate Mass Column Load (2000-2099). This figure represents a time series of sulfate mass loading through the 21st century. Sulfate mass load is represented in units of kg m^{-2} $year^{-1}$ 10^{-6}.

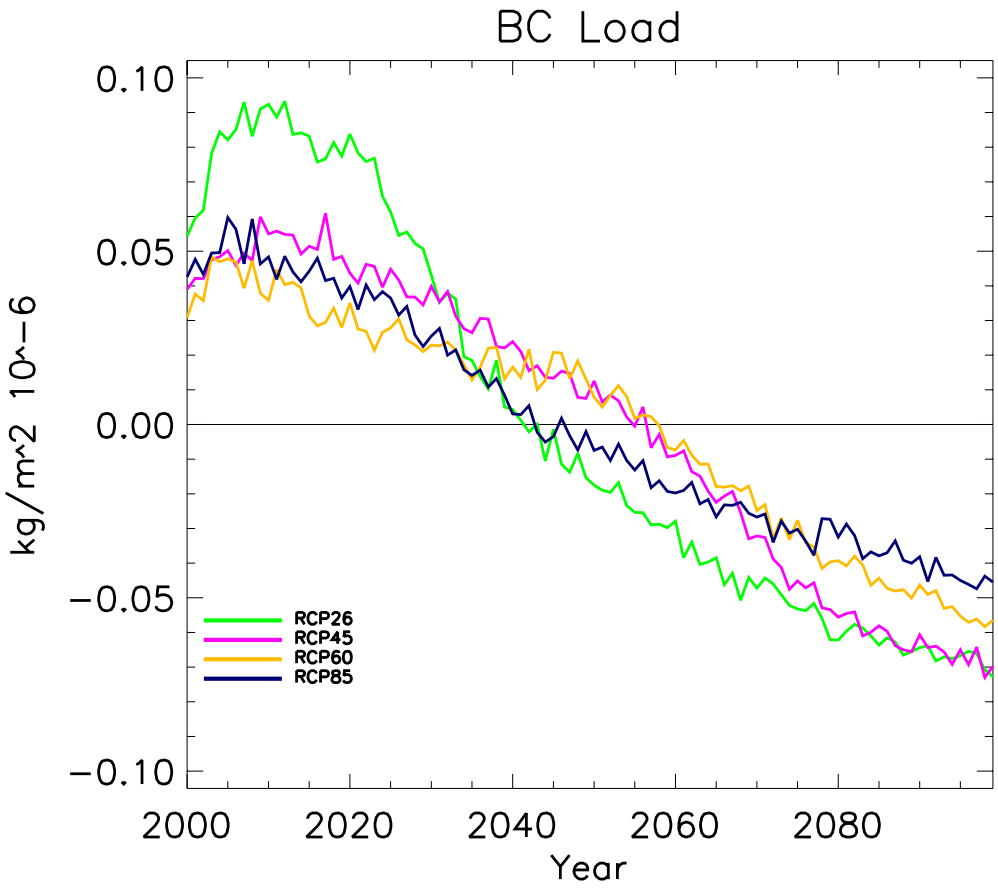

Figure 3. BC Mass Column Load (2000-2099). This figure represents a time series of BC mass loading through the 21st century. BC mass load is represented in units of kg m^{-2} $year^{-1}$ 10^{-6}.

2.3.2 Tropical Expansion Metrics

Three circulation cells characterize Earth's climate: Hadley, Ferrell and Polar cells. More distinctively, these cells can be further categorized as tropical or extra tropical. Unfortunately, the boundaries of the tropical cell are not uniquely defined and vary among scientific disciplines (Seidel et al., 2008). Similar to previous approaches, tropical width is quantified using a variety of metrics (Zhou et al., 2011, Johanson and

Fu, 2009): (1) the latitude of the tropospheric zonal wind maxima (JET); (2) the latitude where the Mean Meridional Circulation (MMC) at 500 hPa becomes zero on the poleward side of the subtropical maximum; (3) the latitude where precipitation minus evaporation (P-E) becomes zero on the poleward side of the subtropical minimum; (4) the latitude of the subtropical precipitation minimum (PMIN) and (5) the latitude of the subtropical cloud cover minimum over oceans (CMIN). Another JET-based measure of tropical width (JET_75) is based on locating the sides of the jet using the 75th percentile of monthly mean zonal wind averaged over the troposphere (850-300 hPa). As used in Allen et al. (2014), the 75th percentile or JET_75 is estimated by sorting the monthly mean zonal wind for each hemisphere from low to high and taking the 0.75(N+1) value, where N is the number of zonal wind values Taking the mid-point yields a time series of monthly jet locations for each hemisphere. In order to calculate MMC, the mass streamfunction (Hartmann**,** 1994) was used, which is defined by calculating the northward mass flux above a particular pressure level, p.

$$\psi = \frac{2\pi\, a\, cos\phi}{g} \int_0^p [v]\, dp \qquad (2.1)$$

For equation 2.1, *v* represents the mean meridional velocity, ø represents the latitude in degrees and g is the gravitational constant. All displacements are estimated by first smoothing the zonal monthly mean of the appropriate field(s) and interpolating to 0.5° resolution using cubic splines. Smoothing was carried out by taking a running mean over ~ 10° of latitude. Changes in tropical width (expansion or contraction) are estimated by

taking a least-squares trend of the seasonal or annual mean time series of each metric.

2.3.3 Statistical Methods

Significance of correlations is estimated assuming a *t*-distribution,

$$t=r/(1-r^2/n-2)^{0.5} \quad (2.2)$$

where *n* is the number of years and *r* is the correlation. Time series are first detrended before estimating correlations. Trend significance is based on a standard t-test, accounting for the influence of serial correlation by using the effective sample size, $n(1-r_1)(1+r_1)^{-1}$, where *n* is the number of years and r_1 is the lag-1 autocorrelation coefficient (Wilks, 2006).

3. Results

Five tropical expansion metrics were analyzed for the 21st century (2000-2099). Analyses of metrics were completed under BC-only, GHG-only, SO_2-only and ALL forcing experiments for each RCP, both on annual and seasonal time scales. Next, these metrics were averaged to give decadal expansion rates for each RCP and values were separated by hemisphere. In all figures containing spatial plots and zonal cross sections, symbols represent significance at the 90% (diamond), 95% (cross) and 99% (dot) confidence level. Tables in section 3.1.1 display decadal expansion rates for each metric averaged annually and seasonally under each RCP obtained from each forcing experiment. Non-bold values, values in bold, bolded values with one asterisk and bolded values with two asterisks represent significance at <90%, 90%, 95% and 99% confidence levels respectively.

3.1 Tropical Expansion Metrics

3.1.1 JET_75 (Tropospheric Jet Displacement)

Decadal expansion rates vary depending on RCP, forcing and season, but generally increase with RCP, regardless of the season and/or forcing (Tables 2-6**).** In addition, only NH expansion rates are shown since this is where the majority of GHG and aerosol emissions originate as well as the bulk of tropical expansion occurs.

Forcing	RCP	JET_75	MMC	P-E	CMIN	PMIN	AVG
ALL	2.6	.0017	-.0119	-.0032	**.0395**	-.0119	.0028
	4.5	**.1262****	**.0718****	**.0794****	**.1479****	**.0684****	.0987
	6.0	**.1411****	**.0846****	**.1055****	**.1549****	**.0792**	.1131
	8.5	**.1847****	**.1394****	**.1500****	**.3105****	**.1368****	.1843
BC	2.6	-.0682	**-.0764****	-.0478	-.0458	-.0673	-.0611
	4.5	.0005	-.0193	-.0197	.0112	-.0224	-.0099
	6.0	.0430	-.0127	.0165	-.0165	-.0127	.0035
	8.5	**-.0931**	-.0404	-.0557	**-.0461**	**-.0616***	-.0594
GHG	2.6	-.0130	-.0224	-.0325	.0077	-.0517	-.0224
	4.5	**.0752**	.0229	.0357	**.0946****	.0011	.0459
	6.0	.0632	.0204	**.0552***	**.0682***	.0238	.0461
	8.5	**.1023***	**.0671****	**.0796****	**.1796****	.0496	.0956
SO_2	2.6	.0089	**.0516****	.0209	**.0681***	**.0828***	.0465
	4.5	**.1382****	**.0909****	**.0931****	**.1407****	**.1161****	.1158
	6.0	**.1213****	**.0724****	**.0612***	**.0778***	**.0949****	.0855
	8.5	**.0956**	**.0799****	**.0690**	**.1035****	**.1023***	.0901

Table 2. Annual mean NH Expansion Rates. The values in this table represent expansion rates for each metric, including an average off all metrics (AVG) for each RCP under various forcing experiments. Units are in º latitude decade^{-1}

Forcing	RCP	JET_75	MMC	P-E	CMIN	PMIN	AVG
ALL	2.6	.0420	-.0148	-.0058	.0883	.0093	.0238
	4.5	**.1432****	**.0825***	.0441	**.2224****	**.1004***	.1185
	6.0	**.1254****	**.0799**	.0721	**.2194****	**.1430****	.1280
	8.5	**.1922****	**.1380****	.0437	**.4381****	**.2348****	.2094
BC	2.6	-.0410	**-.1311****	-.0599	-.0478	-.0601	-.0679
	4.5	.0464	-.0179	-.0351	.0049	.0197	.0036
	6.0	-.0084	-.0622	.0114	-.0401	.0391	-.0121
	8.5	-.0739	-.0407	-.0842	-.0382	-.0259	-.0526
GHG	2.6	.0099	-.0350	-.0799	.0438	-.0754	-.0273
	4.5	.0954	.0258	-.0077	**.1913****	.0397	.0689
	6.0	.0968	.0049	.0143	.1046	**.0807**	.0603
	8.5	**.1489***	**.0904**	-.0329	**.3299****	**.2116****	.1496
SO_2	2.6	.0393	.0623	.0199	**.1524***	.0408	.0629
	4.5	**.1734***	.0710	**.1048**	**.1920****	.0609	.1204
	6.0	**.1301***	**.0948***	.1031	.0448	**.1047**	.0955
	8.5	**.1108**	**.0893**	.0777	**.1454**	**.1586****	.1164

Table 3. NH Expansion Rates averaged for summer months. The values in this table represent expansion rates for each metric, including an average off all metrics (AVG) for each RCP under various forcing experiments. Units are in º latitude decade^{-1}

Forcing	RCP	JET_75	MMC	P-E	CMIN	PMIN	AVG
ALL	2.6	-.0049	.0023	.0092	.0058	.0134	.0051
	4.5	**.1387***	**.0554***	**.0964****	**.1012****	**.1384****	.1060
	6.0	**.2181****	**.0847****	**.1475****	**.0837****	**.0937****	.1255
	8.5	**.2136****	**.1203****	**.2027****	**.1101****	**.1288****	.1551
BC	2.6	-.0792	-.0201	-.0382	-.0531	-.0462	-.0474
	4.5	-.0122	-.0283	-.0123	**.0697**	.0583	.0150
	6.0	**.1091**	.0488	**.0602**	.0034	.0225	.0488
	8.5	-.0884	-.0298	-.0582	-.0417	-.0371	-.0511
GHG	2.6	-.0376	-.0081	-.0227	-.0345	-.0324	-.0271
	4.5	.0423	-.0131	.0392	**.0736***	.0469	.0378
	6.0	**.1728***	.0552	**.1245****	.0425	.0489	.0888
	8.5	.0902	**.0545**	**.1223****	**.0636**	.0002	.0661
SO_2	2.6	**-.1398**	.0005	-.0248	-.0231	.0428	-.0291
	4.5	**.1403****	**.0791****	**.0890****	**.0992****	**.1938****	.1205
	6.0	**.1802****	**.0792****	**.0881****	**.0609**	**.0889***	.0994
	8.5	.0752	.0492	**.0720**	-.0205	**.0944**	.0541

Table 4. NH Expansion Rates averaged for winter months. The values in this table represent expansion rates for each metric, including an average off all metrics (AVG) for each RCP under various forcing experiments. Units are in º latitude decade^{-1}

Forcing	RCP	JET_75	MMC	P-E	CMIN	PMIN	AVG
ALL	2.6	-.0646	**-.0529***	-.0367	.0515	-.0840	-.0373
	4.5	**.1570****	.0254	**.0622****	**.1346****	.0078	.0774
	6.0	**.1329***	**.0512**	**.0829****	**.1482****	.0086	.0848
	8.5	**.2590****	**.1253****	**.1768****	**.3999****	.0605	.2043
BC	2.6	-.1531	**-.0938***	-.0680	-.0292	-.1443	-.0977
	4.5	-.0219	-.0316	-.0323	-.0105	-.0967	-.0299
	6.0	.0666	-.0245	-.0129	-.0723	-.1216	-.0329
	8.5	-.1022	-.0307	-.0362	-.0148	**-.1395**	-.0647
GHG	2.6	-.0290	-.0333	-.0069	.0462	-.0768	-.0199
	4.5	.1245	.0018	.0283	.0756	-.0648	.0331
	6.0	.0494	.0063	.0421	**.0819**	-.0301	.0299
	8.5	**.2050***	.0752	**.1314***	**.1753****	-.0408	.1092
SO_2	2.6	-.0024	.0124	.0006	.0878	.0901	.0377
	4.5	.1235	.0315	.0441	**.1338****	.0471	.0760
	6.0	.0305	-.0043	-.0276	.0207	-.0170	.0005
	8.5	**.2004****	**.0962***	**.0880***	**.2018****	.0559	.1285

Table 5. NH Expansion Rates averaged for spring months. The values in this table represent expansion rates for each metric, including an average off all metrics (AVG) for each RCP under various forcing experiments. Units are in º latitude decade^{-1}

Forcing	RCP	JET_75	MMC	P-E	CMIN	PMIN	AVG
ALL	2.6	.0413	.0238	.0269	.0079	-.0193	.0162
	4.5	.0632	**.1208****	**.1145****	**.1232***	-.0186	.0806
	6.0	**.0871****	**.1253****	**.1187****	**.1580****	.0733	.1125
	8.5	.0717	.1729	.1738	.2802	.0431	.1484
BC	2.6	-.0057	**-.0639**	-.0290	-.0567	.0269	-.0257
	4.5	-.0541	-.0021	-.0005	-.0196	-.0844	-.0321
	6.0	.0003	-.0125	.0089	.0433	.0311	.0142
	8.5	**-.1075***	**-.0603***	-.0468	**-.0875**	-.0276	-.0659
GHG	2.6	.0031	-.0131	-.0199	-.0256	-.0338	-.0288
	4.5	.0358	**.0737**	**.0824****	.0366	-.0379	.0381
	6.0	-.0671	.0145	.0401	.0442	-.0239	.0016
	8.5	-.0365	.0521	**.0944***	**.1465***	-.0216	.0469
SO_2	2.6	**.1364***	**.1341****	**.0888****	.0590	**.1994****	.1235
	4.5	**.1147***	**.1841****	**.1327****	**.1362**	**.2030***	.1541
	6.0	**.1453****	**.1191****	**.0810****	**.1841****	**.2364****	.1532
	8.5	-.0050	**.0869***	.0374	.0878	.0847	.0583

Table 6. NH Expansion Rates averaged for fall months. The values in this table represent expansion rates for each metric, including an average off all metrics (AVG) for each RCP under various forcing experiments. Units are in º latitude decade^{-1}

Tables 2-6 show that tropical expansion rates in each hemisphere range from ~ -0.15º (contraction) to 0.4º latitude decade^{-1} in the NH through the end of century for the five metrics used in this study. Figure 4 shows a zonal cross-section of 21st century, monthly-averaged tropospheric decadal zonal wind patterns for RCP 6.0 under each forcing experiment. Looking at future changes in the latitude of climatological temperature gradient (dT_dY) maxima under the same scenario can further exemplify poleward tropospheric jet displacement (Figures 5 & 6).

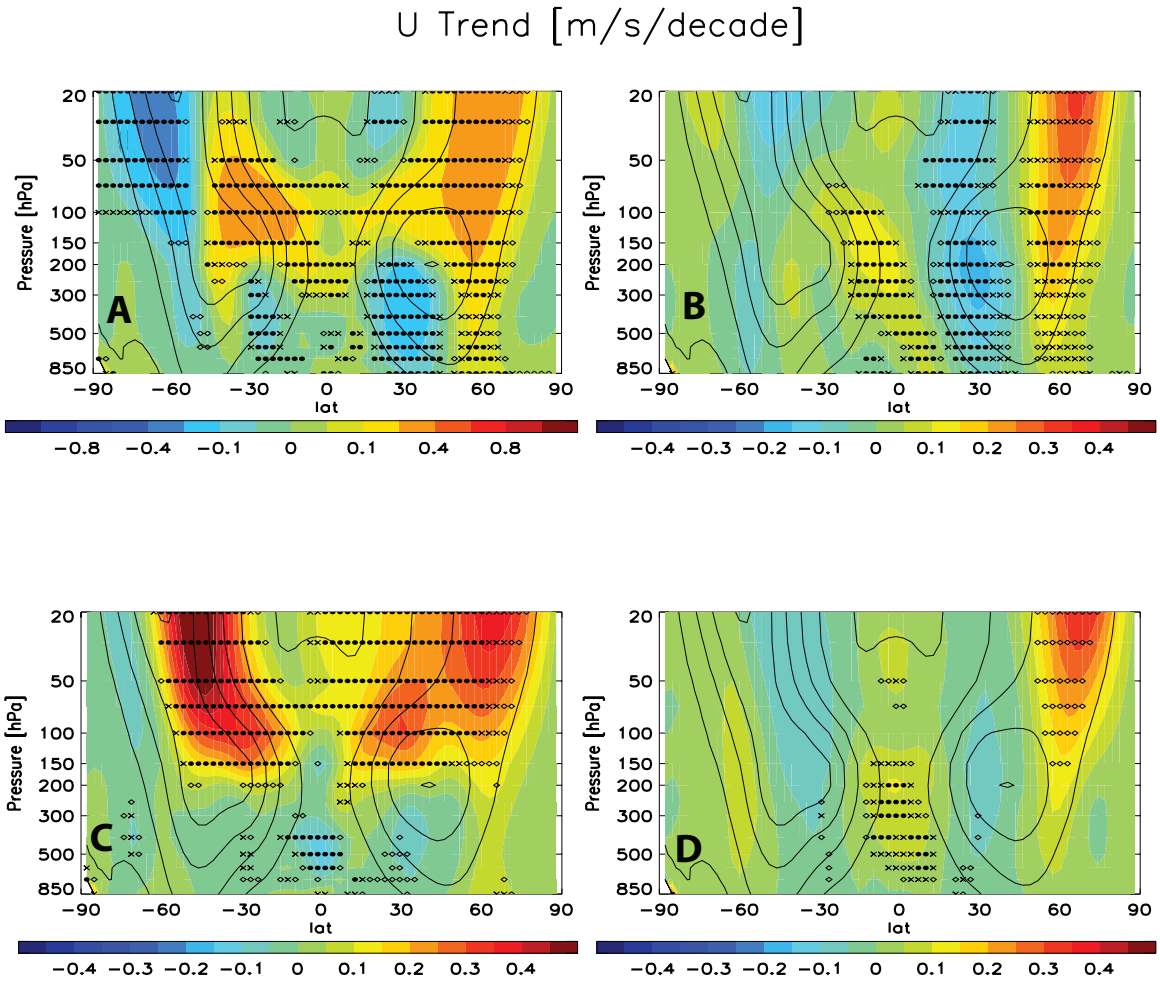

Figure 4. Zonal annual mean zonal wind (U) trends for RCP 6.0. (A) ALL forcing, (B) SO_2 forcing, (C) GHG forcing and (D) BC forcing experiments. Symbols represent trend significance at the 90% (diamond), 95% (cross) and 99% (dot) confidence level, accounting for autocorrelation.

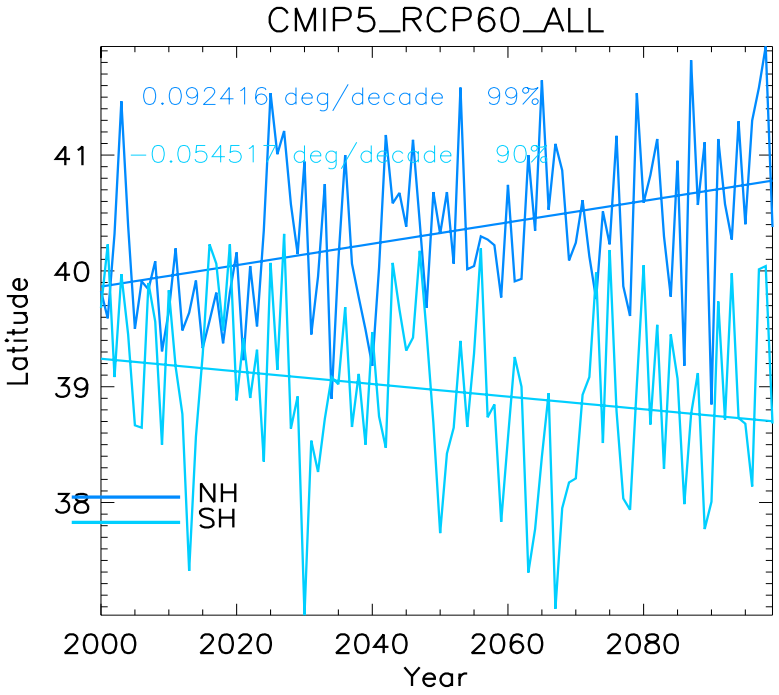

Figure 5. Annual mean time series of tropospheric dT_dY maximum for RCP 6.0. Yearly values represent the latitude with maximum temperature displacement from the previous latitude point.

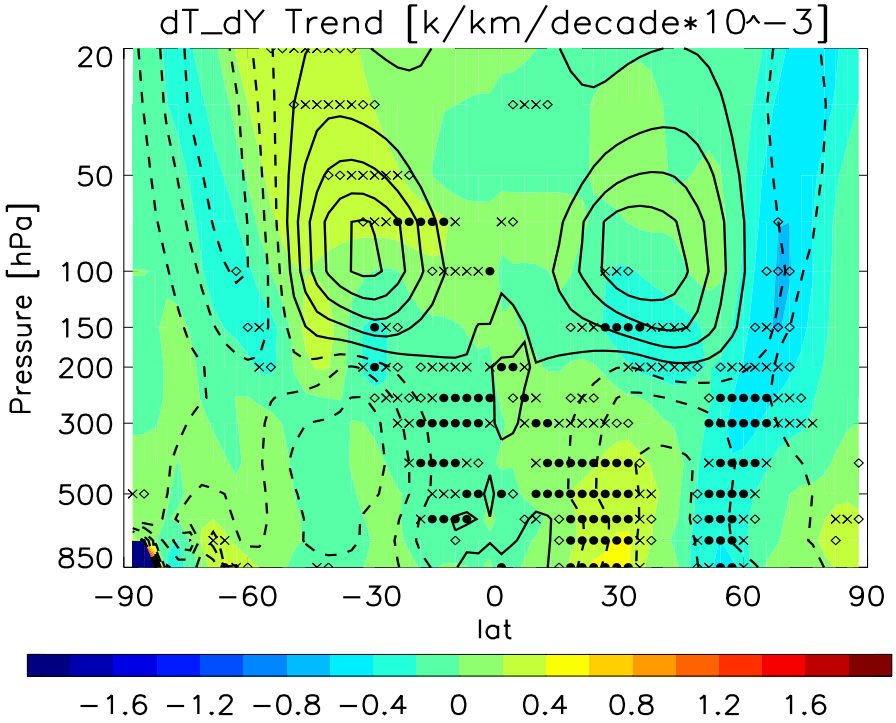

Figure 6. Zonal Annual mean dT_dY trend for RCP6.0 under SO_2 forcing experiment. Symbols represent trend significance at the 90% (diamond), 95% (cross) and 99% (dot) confidence level, accounting for autocorrelation

3.1.2 Mean Meridional Circulation

As with section 3.1.1, expansion rates are generally increasing with RCP. Figure 7 shows the 21st century climatology of zonally averaged annual mean meridional circulation under RCP 8.5 for each forcing experiment. The focus of the results in this section is on the 25-year trends. These results suggest that regions of Hadley cell subsidence will shift poleward.

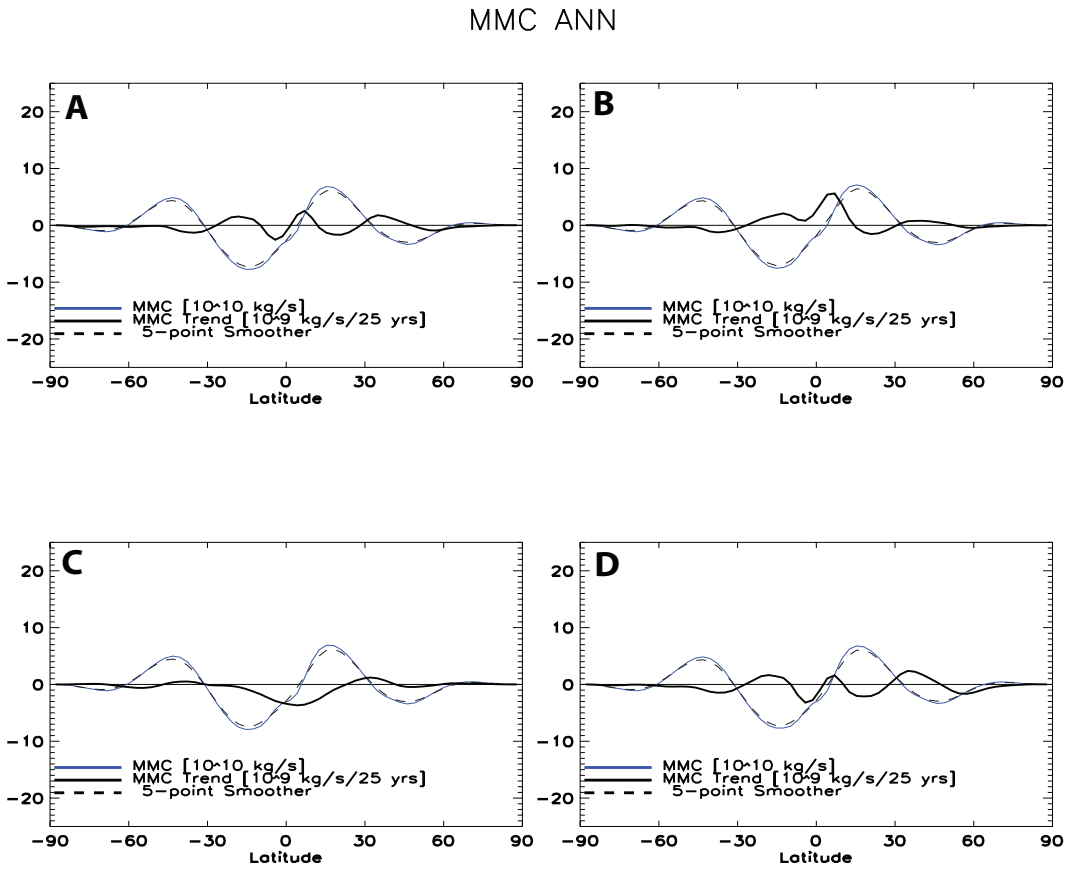

Figure 7. MMC climatology under RCP 8.5. (A) ALL forcing, (B) SO_2 forcing, (C) GHG forcing and (D) BC forcing experiments.

3.1.3 Precipitation-Evaporation (P-E)

Spatial distributions of the change in P-E for BC-only, GHG-only and SO_2-only experiments under RCP 6.0 during winter months are shown in figure 8. The reason for choosing winter months is because this season shows the largest rate of expansion in the NH for this metric. GHG-only and SO_2-only experiments portray evaporation dominance in subtropical (subsidence) regions. Figure 9 shows the zonally averaged annual and winter climatology of P-E under RCP 4.5 and 6.0 for the ALL-forcing experiment. Panels A & C from this figure show an increasing trend in precipitation rates near the equator, ~15ºN-15ºS, and evaporation increasing poleward through the subtropics. As stated in section 3.1.2, the main focus of this figure is on the 25-year trends. The zonal plots within this figure show subtropical regions becoming drier and this trend of evaporation dominance shifting poleward.

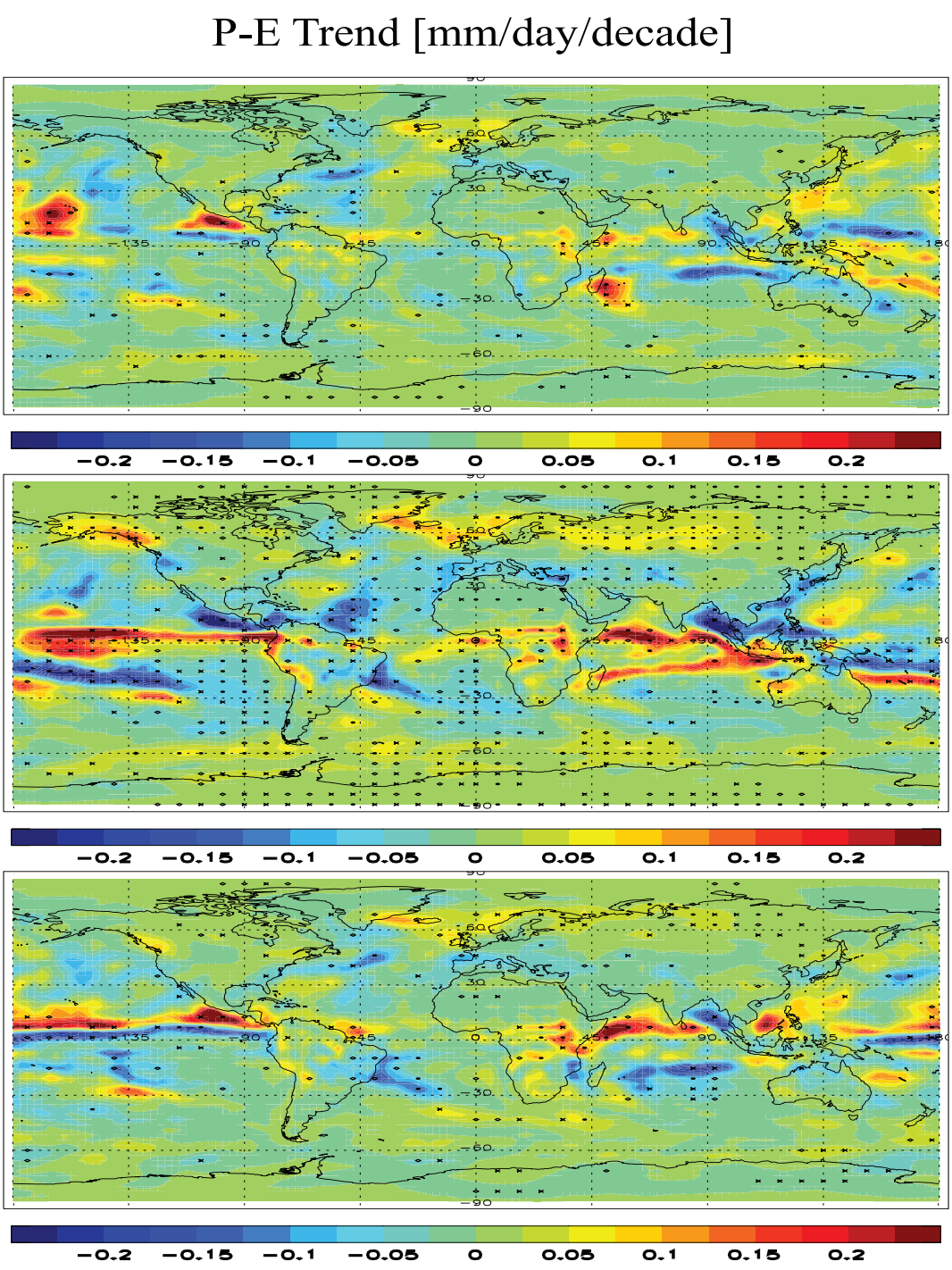

Figure 8. 21st Century spatial P-E trends under RCP 6.0 averaged for winter months. This figure represents BC forcing (top), GHG forcing (middle) and SO_2 forcing (bottom) experiments. Symbols represent trend significance at the 90% (diamond), 95% (cross) and 99% (dot) confidence level, accounting for autocorrelation.

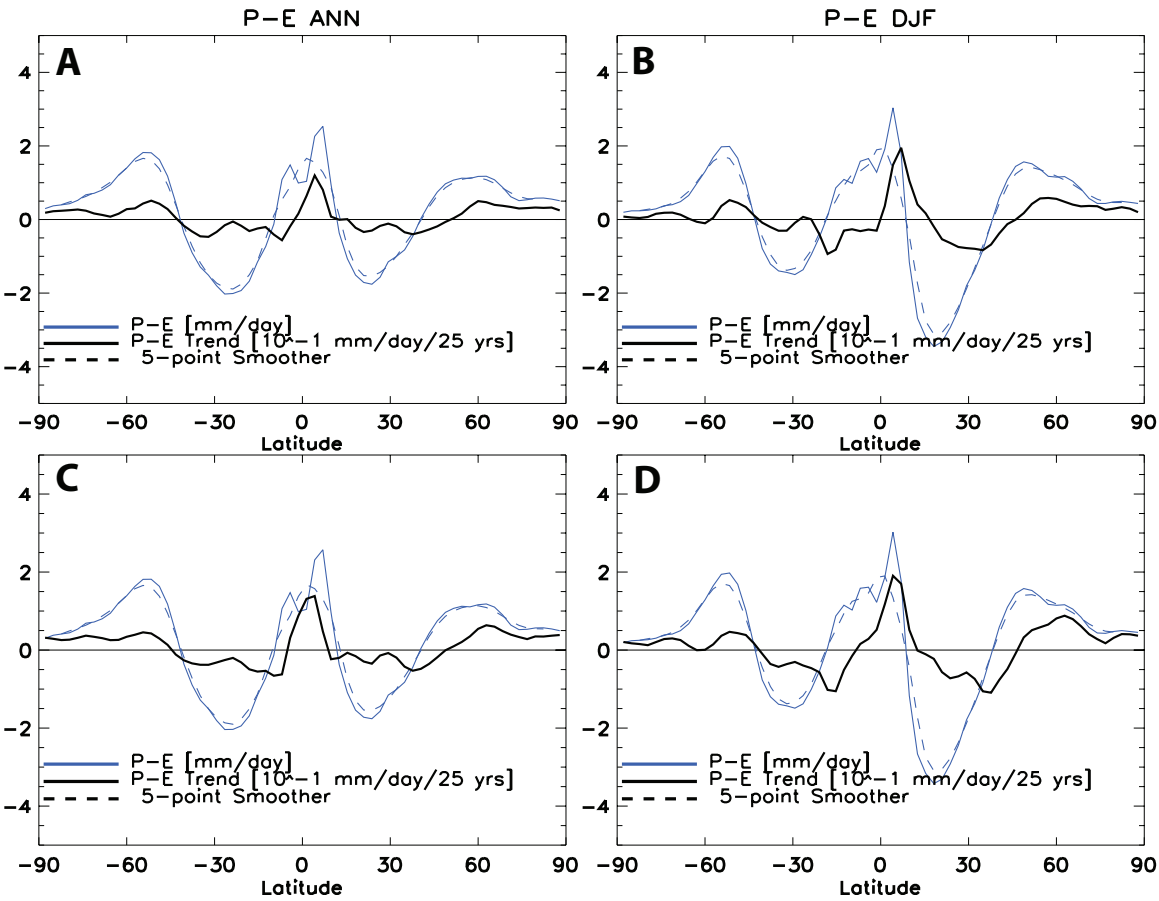

Figure 9. P-E climatology. Panels A & C represent annually averaged climatology data under RCP 4.5 and 6.0 respectively. Panel's B & D represent climatology data under RCP 4.5 and 6.0 for winter month respectively. All panels obtained from the ALL forcing experiment.

3.1.4 Minimum Cloud Coverage (CLT)

Future changes in minimum cloud coverage yields the largest range of expansion among all tropical expansion metrics. As described in section 3.1.3, subtropical regions are projected to experience increased evaporation through the 21st century. Therefore, these subsidence regions will contain less precipitable water, and consequently, a decrease in cloud coverage. This relation will be further discussed in chapter 4. Figure 10

represents annually averaged, vertically integrated cloud coverage under RCP 6.0 for GHG –only (top) and SO_2-only (bottom) experiments.

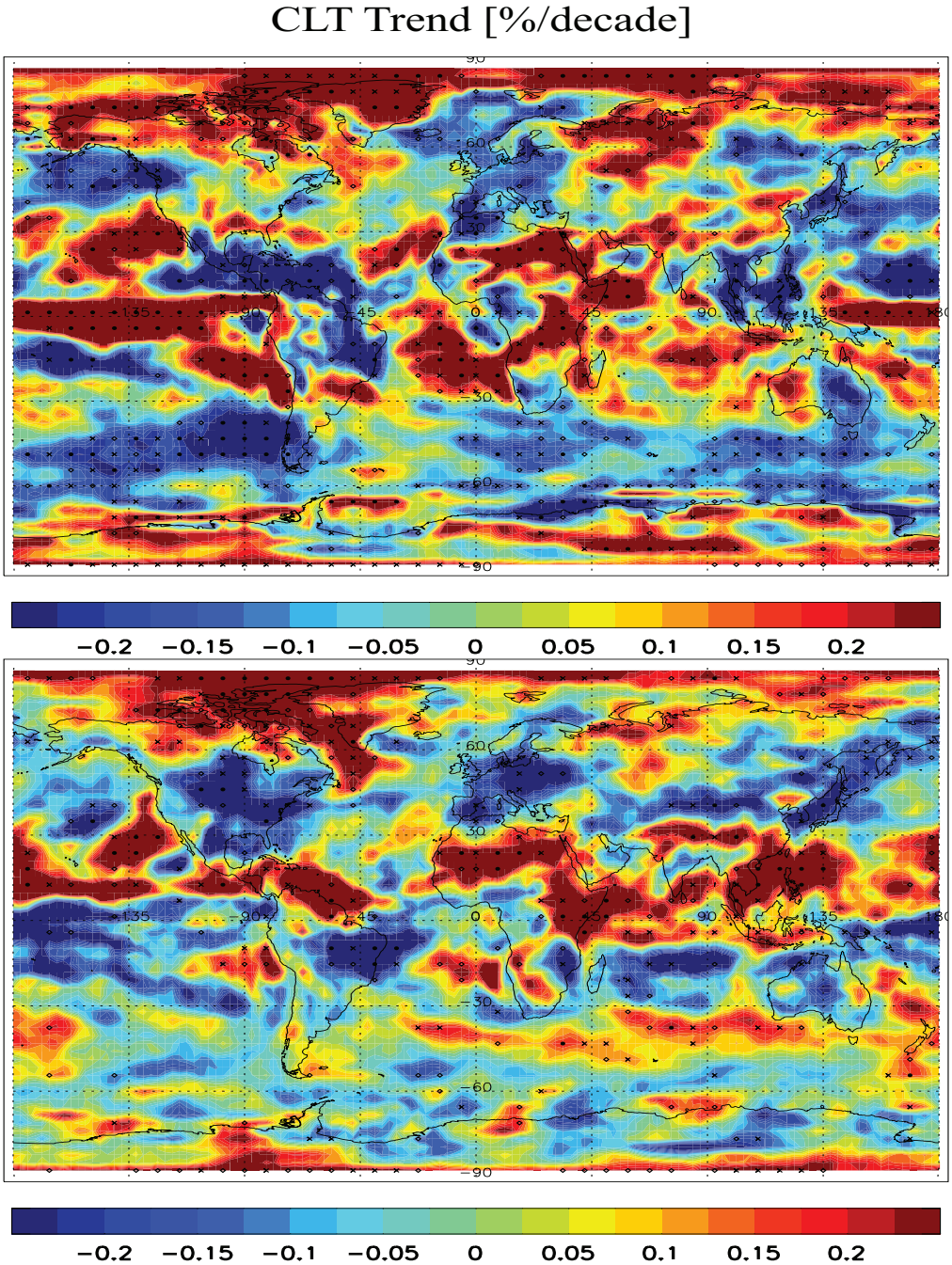

Figure 10. 21st Century annual mean spatial CLT trends under RCP 6.0. GHG (top) and SO_2 (bottom) forcing experiments. Symbols represent trend significance at the 90% (diamond), 95% (cross) and 99% (dot) confidence level, accounting for autocorrelation.

3.1.5 Precipitation Minimum (PMIN)

According to table 2, SO_2 forcing accounts for the most expansion associated with the precipitation minimum metric. Figure 11 shows spatial distributions of estimated surface precipitation changes for BC-only, GHG-only and SO_2-only experiments under RCP 8.5 for the 21st century during summer months. The top panel (SO_2-only) shows the most reduction in precipitation, which primarily occurs in the Southern Hemisphere, middle panel (GHG-only) shows a more uniform change and bottom panel (BC-only) shows minimal decreases in both hemispheres.

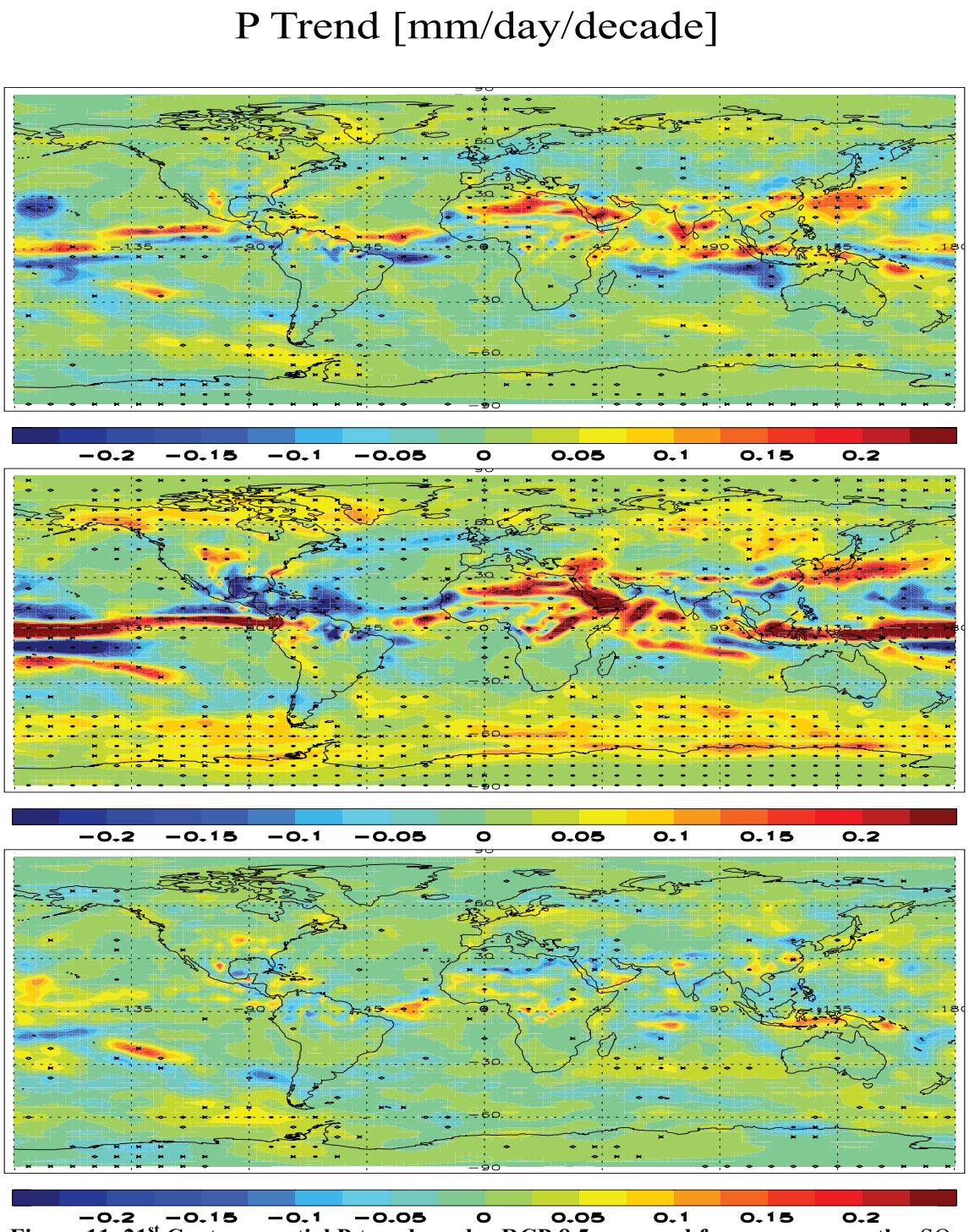

Figure 11. 21st Century spatial P trends under RCP 8.5 averaged for summer months. SO_2 (top), GHG (middle) and BC (bottom) forcing experiments. Symbols represent trend significance at the 90% (diamond), 95% (cross) and 99% (dot) confidence level, accounting for autocorrelation.

3.2 RCP Analysis

The RCP-based expansion rates were calculated for each forcing. Figure 12 shows box plots that represent annually averaged RCP-based expansion rates for each forcing experiment. As expected, expansion values increase with RCP. The mean values are represented with a black line, with upper and lower values reflecting +/- twice the standard error, $2 * \frac{\sigma}{\sqrt{n}}$, where σ is the standard deviation of the metrics and *n* is the number of metrics. Most values obtained from BC-only forcing experiments yielded negligible contraction of tropical belt width (Figure 12). Tables 7, 8 and 9 represent the values obtained from these boxplots, including data from seasonal averages.

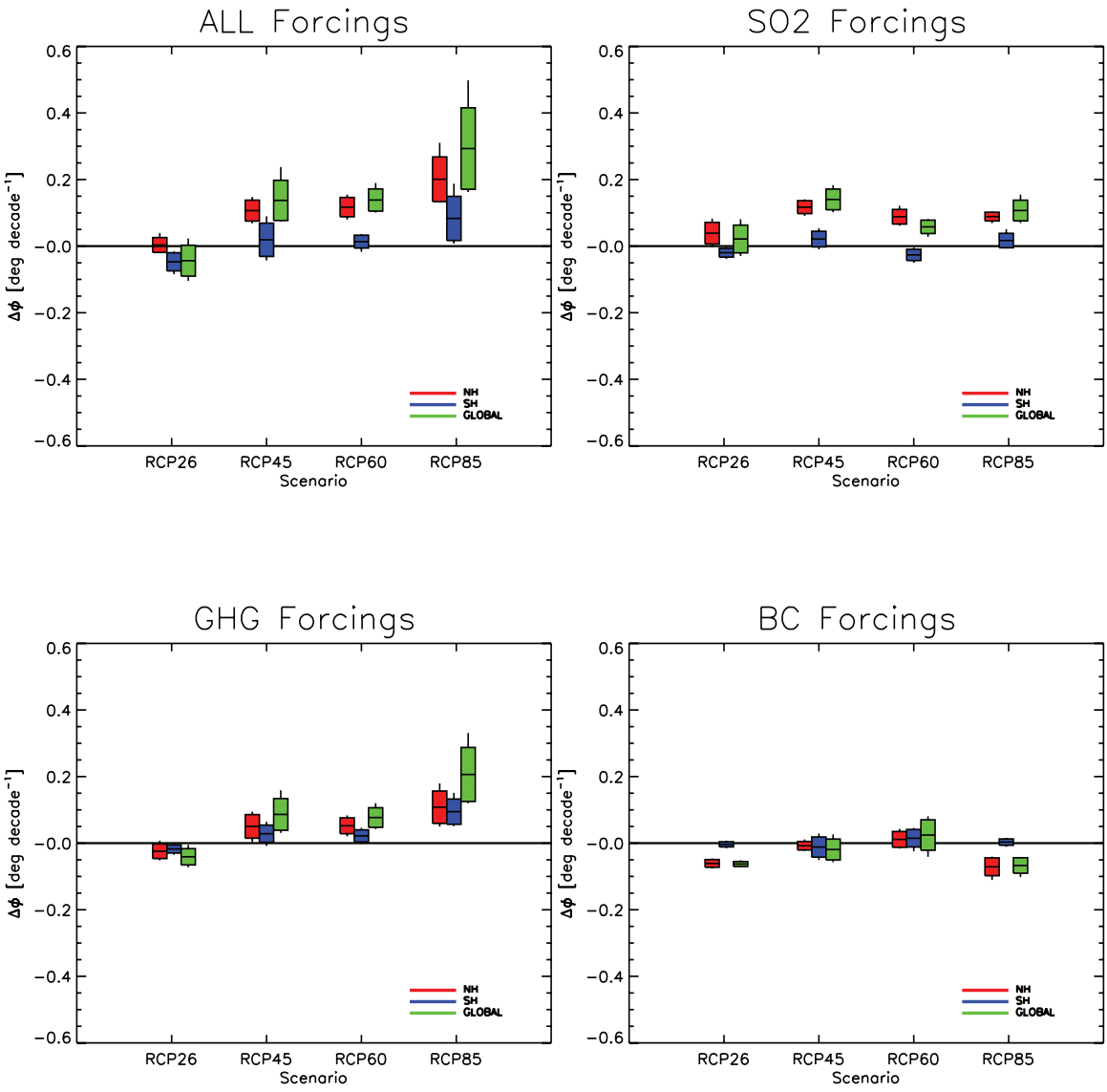

Figure 12. Annual mean decadal expansion rates through the 21ST century under all RCPs for each forcing experiment. All 5 metrics are averaged under each RCP. Boxes show the mean response (center line) and its 2σ uncertainty. Whiskers represent the maximum and minimum values of metrics used to make each box.

FORCING	SEASON	RCP2.6	RCP4.5	RCP6.0	RCP8.5
ALL	ANN	.0034 +/- .0023	.1067 +/- .0315	.1172 +/- .0290	.2009 +/- .0671
	JJA	.0310 +/- .0384	.1286 +/- .0653	.1343 +/- .0548	.2236 +/- .1426
	DJF	-.0113 +/- .0265	.1039 +/- .0315	.1456 +/- .0548	.1588 +/- .0399
	MAM	-.0306 +/- .0507	.1094 +/- .0837	.0931 +/- .0583	.2262 +/- .1257
	SON	.0124 +/- .0222	.0659 +/- .0545	.1047 +/- .0377	.1454 +/- .0895
GHG	ANN	-.0243 +/- .0219	.0503 +/- .0354	.0522 +/- .0238	.1079 +/- .0487
	JJA	-.0184 +/- .0476	.0781 +/- .0733	.0592 +/- .0385	.1518 +/- .1308
	DJF	-.0405 +/- .0280	.0395 +/- .0337	.1342 +/- .0880	.0652 +/- .0441
	MAM	-.0215 +/- .0450	.0478 +/- .0789	.0318 +/- .0415	.1448 +/- .1331
	SON	-.0140 +/- .0263	.0306 +/- .0445	-.0120 +/- .0454	.0445 +/- .0697
BC	ANN	-.0609 +/- .0116	-.0078 +/- .0127	.0113 +/- .0237	-.0709 +/- .0267
	JJA	-.0664 +/- .0407	.0063 +/- .0299	.0096 +/- .0373	-.0561 +/- .0224
	DJF	-.0457 +/- .0221	.0040 +/- .0481	.0507 +/- .0386	-.0839 +/- .0558
	MAM	-.1003 +/- .0479	-.0149 +/- .0586	.0029 +/- .0983	-.0720 +/- .0471
	SON	-.0265 +/- .0350	-.0389 +/- .0319	.0034 +/- .0310	-.0698 +/- .0301
SO_2	ANN	.0388 +/- .0326	.1171 +/- .0194	.0883 +/- .0220	.0887 +/- .0131
	JJA	.0723 +/- .0496	.1267 +/- .0504	.0940 +/- .0313	.1178 +/- .0303
	DJF	-.0797 +/- .1082	.1242 +/- .0438	.1141 +/- .0457	.0360 +/- .0490
	MAM	.0413 +/- .0366	.0898 +/- .0469	.0008 +/- .0216	.1619 +/- .0871
	SON	.1257 +/- .0509	.1500 +/- .0364	.1492 +/- .0584	.0443 +/- .0386

Table 7. NH annual and seasonal expansion rates under each RCP. These values represent mean response +/- 2σ uncertainty. Units are in º decade^{-1}

FORCING	SEASON	RCP2.6	RCP4.5	RCP6.0	RCP8.5
ALL	ANN	-.0471 +/- .0272	.0191 +/- .0500	.0136 +/- .0193	.0833 +/- .0662
	JJA	-.0069 +/- .0183	.0416 +/- .0402	.0284 +/- .0593	.0848 +/- .0401
	DJF	-.1136 +/- .0397	-.0439 +/- .0303	-.0312 +/- .0294	.0578 +/- .0514
	MAM	-.0169 +/- .0267	.0897 +/- .0767	.0757 +/- .0352	.1369 +/- .0818
	SON	-.0479 +/- .0407	-.0011 +/- .0820	.0058 +/- .0585	.0488 +/- .1098
GHG	ANN	-.0175 +/- .0122	.0283 +/- .0259	.0218 +/- .0182	.0946 +/- .0379
	JJA	-.0349 +/- .0333	-.0151 +/- .0563	-.0391 +/- .0689	.0900 +/- .0525
	DJF	-.0135 +/- .0143	.0321 +/- .0136	.0732 +/- .0240	.1029 +/- .0379
	MAM	.0171 +/- .0304	.0923 +/- .0753	.0363 +/- .0208	.1223 +/- .0386
	SON	-.0388 +/- .0242	.0232 +/- .0617	.0010 +/- .0509	.0521 +/- .0678
BC	ANN	-.0036 +/- .0077	-.0117 +/- .0302	.0147 +/- .0263	.0032 +/- .0095
	JJA	-.0319 +/- .0220	-.0225 +/- .0606	.0037 +/- .0692	.0095 +/- .0701
	DJF	.0089 +/- .0131	.0276 +/- .0329	.0239 +/- .0398	.0607 +/- .0225
	MAM	-.0209 +/- .0236	.0264 +/- .0848	.0463 +/- .0436	-.0531 +/- .0441
	SON	.0159 +/- .0187	-.0616 +/- .0463	.0019 +/- .0114	-.0023 +/- .0212
SO_2	ANN	-.0198 +/- .0133	.0213 +/- .0234	-.0263 +/- .0169	.0168 +/- .0217
	JJA	-.0116 +/- .0162	.0157 +/- .0237	-.0467 +/- .0535	.0081 +/- .0670
	DJF	-.0237 +/- .0169	.0219 +/- .0284	.0136 +/- .0305	.0565 +/- .0192
	MAM	-.0457 +/- .0220	.0127 +/- .0581	-.0053 +/- .0197	.0145 +/- .0258
	SON	.0064 +/- .0347	.0374 +/- .0491	-.0727 +/- .0522	-.0267 +/- .0235

Table 8. SH annual and seasonal expansion rates under each RCP. These values represent mean response +/- 2σ uncertainty. Units are in º decade^{-1}

FORCING	SEASON	RCP2.6	RCP4.5	RCP6.0	RCP8.5
ALL	ANN	-.0437 +/- .0463	.1374 +/- .0603	.1385 +/- .0333	.2932 +/- .1224
	JJA	.0279 +/- .0418	.1727 +/- .0680	.1568 +/- .0521	.3278 +/- .1487
	DJF	-.1265 +/- .0633	.0716 +/- .0355	.1112 +/- .0369	.2144 +/- .0445
	MAM	-.0435 +/- .0713	.1895 +/- .1059	.1756 +/- .0683	.3708 +/- .1918
	SON	-.0339 +/- .0305	.0779 +/- .1109	.1150 +/- .0898	.1999 +/- .1896
GHG	ANN	-.0410 +/- .0243	.0863 +/- .0476	.0769 +/- .0294	.2063 +/- .0810
	JJA	-.0532 +/- .0267	.0638 +/- .0404	.0324 +/- .0529	.2557 +/- .1277
	DJF	-.0554 +/- .0391	.0705 +/- .0365	.2074 +/- .1096	.1715 +/- .0505
	MAM	-.0045 +/- .0748	.1277 +/- .1192	.0647 +/- .0574	.2577 +/- .1531
	SON	-.0448 +/- .0357	.0594 +/- .0662	-.0099 +/- .0939	.0965 +/- .1354
BC	ANN	-.0627 +/- .0075	-.0190 +/- .0313	.0244 +/- .0457	-.0671 +/- .0232
	JJA	-.0945 +/- .0262	-.0099 +/- .0600	-.0072 +/- .0881	-.0561 +/- .0224
	DJF	-.0329 +/- .0225	.0418 +/- .0541	.0708 +/- .0697	-.0189 +/- .0610
	MAM	-.1224 +/- .0617	.0006 +/- .0965	.0440 +/- .0785	.1177 +/- .0793
	SON	-.0118 +/- .0442	-.0972 +/- .0647	.0029 +/- .0388	-.0658 +/- .0303
SO_2	ANN	.0215 +/- .0417	.1403 +/- .0312	.0579 +/- .0202	.1071+/- .0310
	JJA	.0646 +/- .0611	.1401 +/- .0446	.0438 +/- .0794	.1395 +/- .0623
	DJF	-.0992 +/- .1158	.1473 +/- .0605	.1167 +/- .0547	.0982 +/- .0562
	MAM	-.0039 +/- .0348	.1064 +/- .0824	-.0064 +/- .0345	.1713 +/- .0833
	SON	.1351 +/- .0803	.1874 +/- .0829	.0789 +/- .0878	.0207 +/- .0556

Table 9. Global (NH+SH) annual and seasonal expansion rates under each RCP. These values represent mean response +/- 2σ uncertainty. Units are in º decade^{-1}

3.3 21st Century Temperature Analysis

Changes in tropospheric temperature (T) were analyzed for each RCP and forcing experiment. Figure 13 shows zonal cross-sections of 21st century annually averaged temperature trends under RCP 6.0 for BC-only, SO_2-only and GHG-only forcing experiments respectively. The primary areas on warming fall within the NH for the SO_2 forcing experiment. There is a more uniform warming (cooling) trend for the GHG (BC) forcing experiment. In addition to global representations of temperature, annual mean changes in NH tropospheric (850-300 hPa) temperatures through time were also obtained (Figure 14).

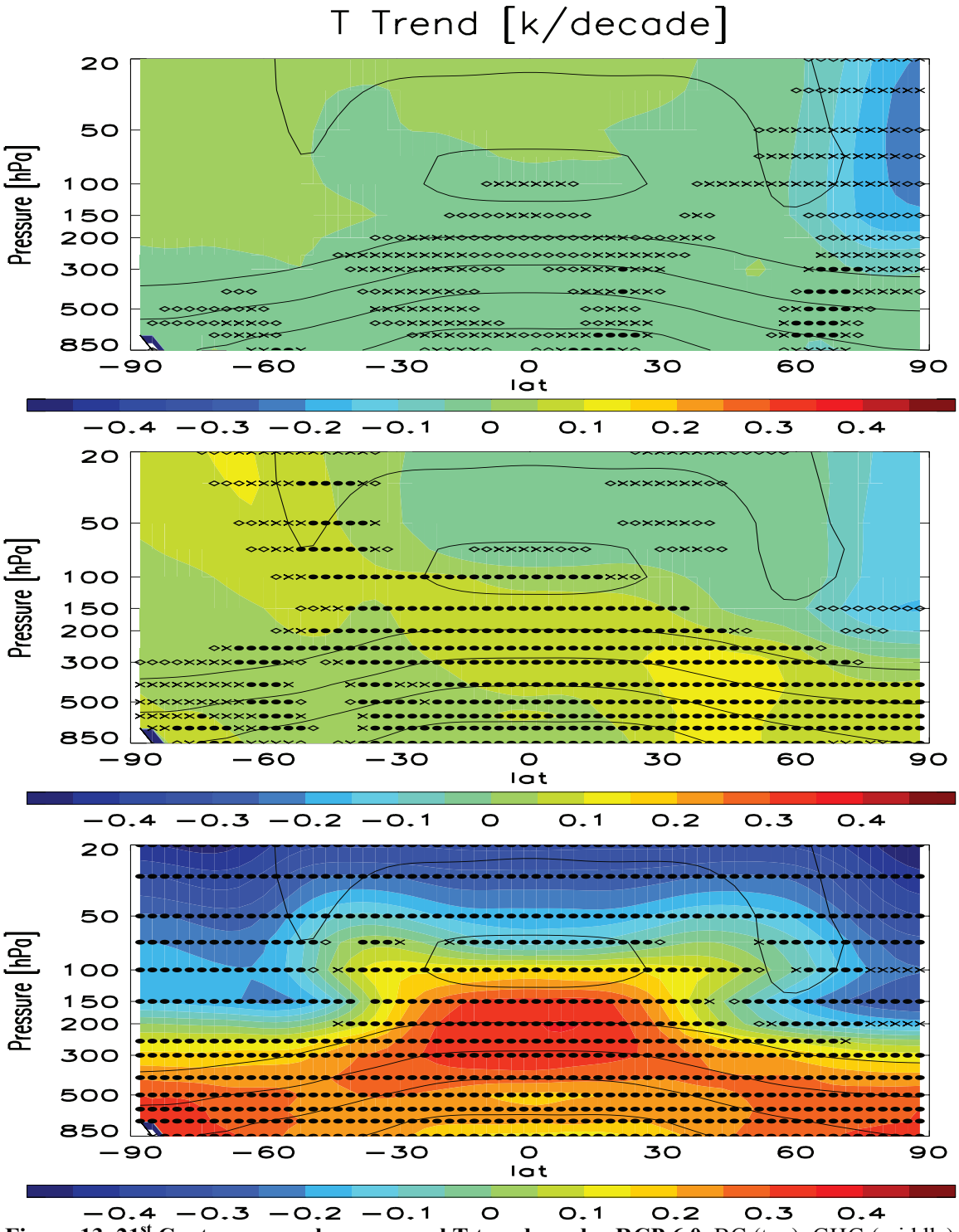

Figure 13. 21st Century annual mean zonal T trends under RCP 6.0. BC (top), GHG (middle) and SO_2 (bottom) forcing experiments. Symbols represent trend significance at the 90% (diamond), 95% (cross) and 99% (dot) confidence level, accounting for autocorrelation.

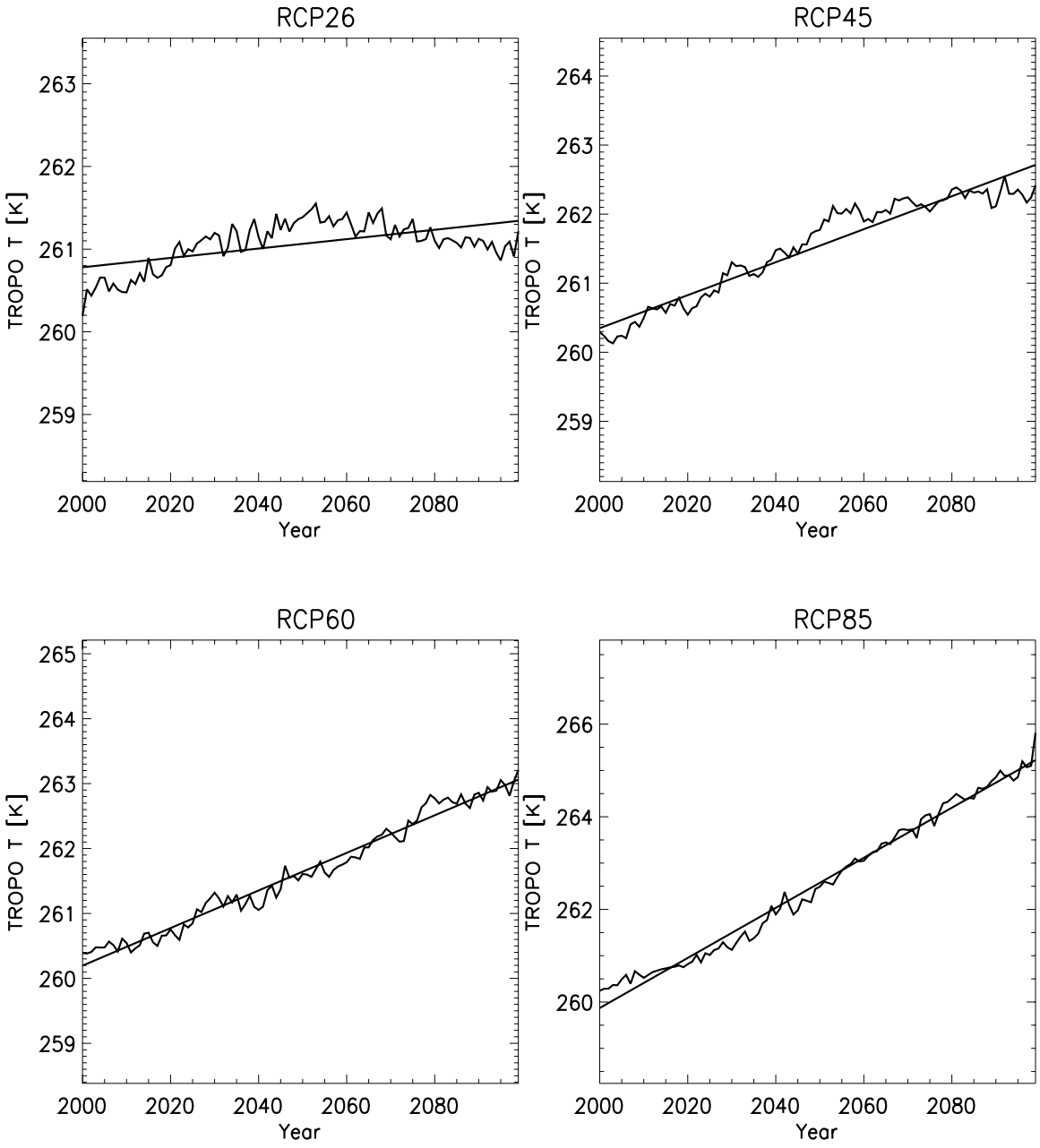

Figure 14. NH tropospheric T time series for each RCP. Units are in º Kelvin and solid line represents linear trend of annual values.

3.4 Sulfates and Tropical Widening

Under RCP 4.5 (RCP6.0) and the ALL forcing experiment, the tropics expand .14+/-.06º decade^{-1} (.14+/-.03º decade^{-1}) (Table 9), with the majority of that expansion occurring in the NH (Table 7) at values of .11+/-.03º decade^{-1} (.12+/-.03º decade^{-1}). Of this NH value, SO_2 yields considerable tropical expansion at .12+/-.02º decade^{-1} (.09+/-.02º decade^{-1}) while GHG's account for .05+/-.04º decade^{-1} (.05+/-.02). For RCP 8.5, GHG's and SO_2 yield NH tropical expansion at .11+/-.05º decade^{-1} and .09+/-.01º decade^{-1} respectively. Hence, even under the pathway that projects the highest increase in greenhouse emissions, sulfate aerosols drive as much NH tropical expansion as do GHG's. Figure 15 shows the spatial annual trend in sulfur emissions under RCP 6.0. A closer look clearly shows that most of the decrease in SO_2 emissions occurs in the NH. In particular, the signal of this decrease is strongest along the east coast of the United States, Europe and eastern Asia.

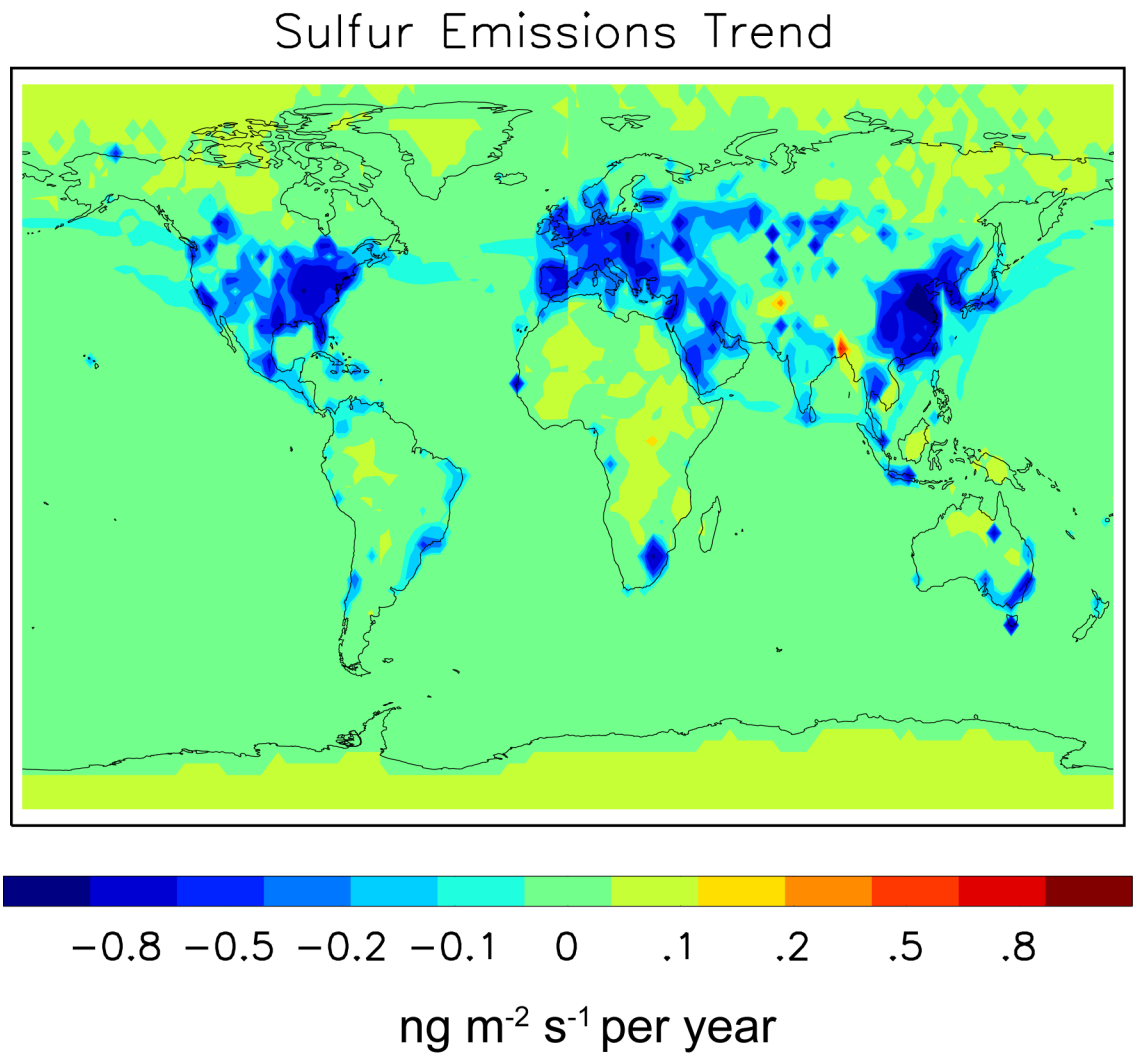

Figure 15. 21st Century annual mean sulfur trend. Reflects emissions of SO_2 and dimethyl sulfide (DMS), the two primary sulfate aerosol precursors.

4. DISCUSSION/CONCLUSION

4.1 Tropical Expansion Mechanisms

Ramanathan et al. (2001) discussed how aerosols directly attenuate surface solar radiation (SSR) by scattering and absorbing solar radiation (direct effect), or indirectly attenuate SSR through their ability to act as cloud condensation nuclei (CCN), thereby increasing cloud reflectivity and lifetime (1^{st} and 2^{nd} indirect effects). Absorbing aerosols, such as black carbon (BC), heat the atmosphere and reduce solar radiation received at the surface dependent on vertical distribution.

The mechanisms driving tropical expansion are not well known. In the case of GHG warming, an increase in subtropical static stability, which reduces baroclinic growth rates and displaces the region of baroclinic instability onset poleward, resulting in tropical expansion. Such heating weakens the climatological temperature gradient on the equatorward flank of the maximum, but strengthens it on the poleward flank. A geostrophic adjustment (thermal wind balance) implies a poleward displacement of the circulation (Allen & Sherwood, 2011).

Reflecting aerosols, including SO_2, prevent solar radiation from reaching the surface due to its high albedo. In particular, anthropogenic sulfate aerosols have been linked to times of global dimming and brightening through an increase and decrease in emissions respectively (Wild, 2012). Thus, future decreases in sulfate aerosol emissions will warm the surface and decrease cloud coverage, which in turn expands tropical belt width. In tropical regions, warming of the surface may lead to convection and precipitation, where as in subtropical regions, warming of the surface can lead to

increased evaporation (rich-gets-richer mechanism). Section 3.4 states that the bulk of the decrease in SO_2 emissions will occur in the NH. These areas collocate with the latitude of meridional temperature gradient maximum and the latitude of the strongest NH jet. Mechanically, SO_2 drives tropical expansion the same way as GHG's. However, unlike GHG's, which warm the planet uniformly, the warming associated with SO_2 decreases across all RCPs will be focused in the NH. This warming leads to a poleward displacement of NH meridional temperature gradient maximum. The jet responds by shifting poleward, consistent with a geostrophic adjustment to the altered meridional temperature gradient and is in accordance with the thermal wind balance.

4.2 General Discussion

Five tropical expansion metrics were analyzed through the 21st century using CAM3. Section 3 shows robust expansion of tropical belt width in the NH, primarily due to changes in GHG and SO_2 emissions. In particular, the future decreases in SO_2 are just as dominant a driver in expanding tropical belt width as future increases in GHG's. Previous studies (Allen et al., 2012) have shown BC to be the main driver in expanding tropical belt width since its emissions were steadily increasing through the late 20th century. With the research shown here, we suggest that future decreases in BC will work against this mechanism (contraction), although the expansion caused by other forcing agents trump whatever effects BC forcing may have. We find that under RCP4.5, the annually-averaged expansion rate of the five metrics (ALL) is 0.09 latitude decade^{-1}, in which, 46.5% is due to GHG forcing and ~47% due to SO_2 forcing. Also, we find that

under RCP8.5, expansion rates for the ALL metric is .18, with GHG and SO_2 forcings responsible for ~ 51% and 49% respectively. This result suggest that changes in SO_2 emissions are just as important in driving NH tropical expansion, even in RCP 8.5, where GHG emissions are largest.

Sulfate aerosols are rather important because of their ability to reflect incoming, shortwave radiation and act as CCN, which leads to cloud development. More so, this research shows that decreases in sulfate emissions will reduce cloud coverage (figure 10), particularly in the NH subtropics. We find that the latitude where cloud coverage is at its minimum yields the largest rate of expansion amongst all metrics. The most NH expansion associated with this metric occurs during summer (~ 0.44º decade^{-1}) and spring (~ 0.40º decade^{-1}) months.

Analysis on zonal wind show a strengthening of westerly atmospheric flow, which is consistent with what Quan et al., 2004 concluded (figure 4). We show that the latitude where meridional temperature gradients reaches it maximum shifts poleward and is indicative of mid-latitude warming, which strengthens the jet in accordance to the thermal wind balance. Temperature changes according to GHG and SO_2 forcing experiments further back up this claim. This finding also implies a poleward shift of the subtropical jet and is indicative of extratropical storm tracks being pushed poleward as well, which in turn may lead to an increase in areas affected by tropical storms (Seidel et al., 2008). Of the four panels shown in figure 4, panel B (SO_2 forcing) shows that SO_2 is the most important forcing agent drives change in zonal wind trends through the 21st century. Panel C (GHG forcing) suggest that future changes in GHG emissions will have

an effect on the main jet stream located at the tropopause. As temperatures increase in the troposphere due to GHG forcing (figure 3), this leads to a strong meridional temperature gradient, which can lead to a stronger zonal stratospheric winds.

Changes in the MMC metric are primarily caused by SO_2 and GHG forcings, regardless of season (tables 2-6). Also, the expansion rates of the MMC metric due to SO_2 are the most statistically significant. Regions in the subtropics that may become exposed to the descending branch of the Hadley cell coincide with evaporation dominance (figure 8). The bulk of this response comes from GHG and SO_2 forcings. As the latitude where MMC=0 extends poleward, the dry zone associated with this subsidence will expand poleward as well and those inhabiting this region will experience less rainfall than traditionally expected.

Data obtained from the P-E metric is consistent with the idea: wet regions get wetter and dry regions become drier, which is due to local thermodynamic and energetic constraints (Held and Solden, 2006). Locally, precipitation could be enhanced in convective regions following the "rich-get-richer mechanism" because gross moist stability is reduced when the increase in moisture is concentrated mainly in the lower troposphere (Zhou et al., 2011; Chou and Neelin, 2004; Chou et al., 2009) The data produced from this metric compliment our findings with minimum cloud coverage. As regions with minimal cloud coverage expand poleward, these same regions may experience large-scale drought. Unfortunately, one shortcoming to note is the increases in precipitation near the Sahara region shown in figure 11. This outcome is unlikely since this region is currently a desert.

We provide evidence that the forcing due to changes in SO_2 emissions are just as important, if not more, than GHG forcings in driving future changes in tropical belt width (figure 12). When comparing the decadal expansion rates, changes due to SO_2 forcings show more certainty. We infer that the bulk of future expansion will occur in the NH based on results shown in section 3.2 under ALL, SO_2 and GHG forcing experiments, where the bulk of the planet's population resides as well as where the most SO_2 emissions originate. Fortunately, projections from RCP 2.6 show contraction of the tropical belt, which should not be harmful to subtropical regions. However, if the projections from the other RCPs play out, then there will be substantial changes in policy for these regions, especially for ones undergoing economic hardship or highly dependent on agricultural practices.

Consistent with previous studies (Gillett and Salzen, 2013; Rotsalyn et al., 2013), projected, progressive decreases in aerosol emissions under the RCP scenarios will drive warming through the 21st century. The rate and magnitude of warming are heavily dependent of RCP. Since sulfate aerosols have a negative radiative forcing, a reduction in emissions may lead to surface warming (Kloster et al., 2010). However, we find that increases in GHG's are more dominant than decreases in sulfate emissions at driving surface warming, with the bulk of extratropical regions warming about 2º-4ºK through the 21st century (figures 13 & 14). Our studies are also consistent with Fu and Lin (2011) whom concluded that decreasing temperature trends in the stratosphere (100 hPa in the tropics and 200 hPa elsewhere) led to a poleward shift of subtropical jets.

4.3 Conclusion

In conclusion, we have diagnosed model simulations in order to understand potential changes in tropical belt width. Following the research done by Allen et al. (2012), which showed that recent (1979-2009) NH tropical expansion was caused by aerosol forcing agents (BC & tropospheric ozone), we quantified changes in tropical belt width through the 21st century. The most important finding is that the aerosol forcing associated with progressive decreases in SO_2 emissions drive as much expansion in the NH as future increases in GHG emissions. According to our findings, SO_2 forcing not only drives as much expansion as GHG forcing, but there is less uncertainty associated with decadal expansion rates. Future changes in expansion rates due to SO_2 forcing under RCPs 4.5, 6.0 and 8.5 show little difference, whereas expansion rates due to GHG forcing steadily increase with RCP. This implies that if future aerosol and GHG emissions follow the trajectory of RCPs 4.5 or 6.0, SO_2 reductions may be more important at driving expansion of tropical belt width relative to GHG increases.

We show that future widening of the tropics will probably be associated with a poleward shift of major extratropical climate zones based on our results displaying a poleward shift of the subtropical jet. Since subtropical dry zones are projected to shift poleward and these areas lay within semi-arid regions, the population will be heavily at risk. While equatorial regions may see an increase in precipitation rates, many other areas are projected to become drier (e.g. SE United States, Western Europe, parts of Central and South America as well as parts of the Atlantic Ocean and Indian Oceans). Of particular importance, these areas lay within the borders of second and third world

countries. A poleward expansion of the tropics will likely bring drier conditions to these heavily populated regions, especially ones highly dependent on water resources and agricultural practices.

Although SO_2 forcing accounts for the bulk of future expansion, we believe that our results underestimate the true magnitude of this forcing since CAM3 does not include aerosol indirect effects. The next step in this research will be to perform the same analysis using multiple models that incorporate aerosol indirect effects (e.g. CAM5) to analyze any similarities and differences amongst models and any deficiencies our results from CAM3 may have. By including aerosol indirect effects, we believe that expansion rates from SO_2 forcing may differ relative to the results presented. Our CAM3 simulation did not include methane emissions. As methane emissions are projected to increase, this can lead to further expansion. Also, the projected decline in aerosol emissions in the IPCC AR5 RCPs is larger than that in prior scenarios (van Vuuren et al., 2011). Therefore, our results may overestimate the magnitude of NH widening through the 21st century. Lastly, some studies (Quan et al., 2014; Allen et al., 2014) suggest that changes in sea surface temperature (SST) are the biggest driver of expansion. The next step for this research should utilize future projections in SST's and how they may potentially affect tropical expansion rates.

References

Allen, R. J., & Sherwood, S. C. (2011). "The impact of natural versus anthropogenic aerosols on atmospheric circulation in the Community Atmosphere Model." *Climate dynamics*, *36*(9-10), 1959-1978.

Allen, R. J., Sherwood, S. C., Norris, J. R., & Zender, C. S. (2012). "Recent Northern Hemisphere tropical expansion primarily driven by black carbon and tropospheric ozone." *Nature*, *485*(7398), 350-354.

Allen, R. J., Norris, J. R., & Kovilakam, M. (2014). "Influence of anthropogenic aerosols and the Pacific Decadal Oscillation on tropical belt width." *Nature Geoscience*, *7*(4), 270-274.

Bond, T. C., & Bergstrom, R. W. (2006). "Light absorption by carbonaceous particles: An investigative review." *Aerosol Science and Technology*, *40*(1), 27-67.

Chou, C., & Neelin, J. D. (2004). "Mechanisms of global warming impacts on regional tropical precipitation." *Journal of climate*, *17*(13).

Chou, C., Neelin, J. D., Chen, C. A., & Tu, J. Y. (2009). "Evaluating the "rich-get-richer" mechanism in tropical precipitation change under global warming." *Journal of Climate*, *22*(8).

Collins, W. D., Rasch, P. J., Boville, B. A., Hack, J. J., McCaa, J. R., Williamson, D. L., ... & Dai, Y. (2004). "Description of the NCAR community atmosphere model (CAM 3.0)." *NCAR Tech. Note NCAR/TN-464+ STR*, 226.

Flanner, M. G., Zender, C. S., Randerson, J. T., & Rasch, P. J. (2007). "Present-day climate forcing and response from black carbon in snow." *Journal of Geophysical Research: Atmospheres (1984–2012)*, *112*(D11).

Flanner, M. G., Zender, C. S., Hess, P. G., Mahowald, N. M., Painter, T. H., Ramanathan, V., & Rasch, P. J. (2009). "Springtime warming and reduced snow cover from carbonaceous particles." *Atmospheric Chemistry and Physics*, *9*(7), 2481-2497.

Fu, Q., & Lin, P. (2011). "Poleward Shift of Subtropical Jets Inferred from Satellite-Observed Lower-Stratospheric Temperatures." *Journal of Climate*, *24*(21).

Gillett, N. P., & Von Salzen, K. (2013). "The role of reduced aerosol precursor emissions in driving near-term warming." *Environmental Research Letters*, *8*(3), 034008.

Hartmann, D. L. (1994). *Global physical climatology* (Vol. 56). Academic press.

Held, Isaac M., and Brian J. Soden. "Robust responses of the hydrological cycle to global warming." *Journal of Climate* 19.21 (2006).

Hu, Y., & Fu, Q. (2007). "Observed poleward expansion of the Hadley circulation since 1979." *Atmospheric Chemistry and Physics*, *7*(19), 5229-5236.

Johanson, C. M., & Fu, Q. (2009). "Hadley cell widening: Model simulations versus observations." *Journal of Climate*, *22*(10).

Kloster, S., Dentener, F., Feichter, J., Raes, F., Lohmann, U., Roeckner, E., & Fischer-Bruns, I. (2010). "A GCM study of future climate response to aerosol pollution reductions." *Climate dynamics*, *34*(7-8), 1177-1194.

Lipscomb, W., & Sacks, W. (2010). The CESM Land Ice Model: Documentation and User's Guide. *Los Alamos National Laboratory*.

Moss, R. H., Edmonds, J. A., Hibbard, K. A., Manning, M. R., Rose, S. K., Van Vuuren, D. P., ... & Wilbanks, T. J. (2010). "The next generation of scenarios for climate change research and assessment." *Nature*, *463*(7282), 747-756.

Nakicenovic, N., & Swart, R. (2000). "Special report on emissions scenarios. *Special Report on Emissions Scenarios", Edited by Nebojsa Nakicenovic and Robert Swart, pp. 612. ISBN 0521804930. Cambridge, UK: Cambridge University Press, July 2000.*, *1*.

Quan, X. W., Hoerling, M. P., Perlwitz, J., Diaz, H. F., & Xu, T. (2013). "How fast are the tropics expanding?". *Journal of Climate*, (2013).

Quan, X. W., Diaz, H. F., & Hoerling, M. P. (2004). "Changes in the tropical Hadley cell since 1950." *The Hadley Circulation: Present, Past, and Future*, 85-120.

Ramanathan, V. C. P. J. K. J. T. R. D., Crutzen, P. J., Kiehl, J. T., & Rosenfeld, D. (2001). "Aerosols, climate, and the hydrological cycle." *science*, *294*(5549), 2119-2124.

Rotstayn, L. D., Collier, M. A., Chrastansky, A., Jeffrey, S. J., & Luo, J. J. (2013). "Projected effects of declining aerosols in RCP4. 5: unmasking global warming?" *Atmospheric Chemistry and Physics*, *13*(21), 10883-10905.

Seidel, D. J., Fu, Q., Randel, W. J., & Reichler, T. J. (2007). "Widening of the tropical belt in a changing climate." *Nature geoscience*, *1*(1), 21-24.

Van Vuuren, D. P., Edmonds, J., Kainuma, M., Riahi, K., Thomson, A., Hibbard, K., ... & Rose, S. K. (2011). "The representative concentration pathways: an overview." *Climatic Change*, *109*, 5-31.

Wild, M. (2012). "Enlightening Global Dimming and Brightening." *Bulletin of the American Meteorological Society*, *93*(1).

Wilks, D. S. (2006). Statistical methods in the atmospheric sciences.

Zhang, G. J., & McFarlane, N. A. (1995). "Sensitivity of climate simulations to the parameterization of cumulus convection in the Canadian Climate Centre general circulation model." *Atmosphere-Ocean*, *33*(3), 407-446.

Zhou, Y. P., Xu, K. M., Sud, Y. C., & Betts, A. K. (2011). "Recent trends of the tropical hydrological cycle inferred from Global Precipitation Climatology Project and International Satellite Cloud Climatology Project data." *Journal of Geophysical Research: Atmospheres (1984–2012)*, *116*(D9).